Research article

Comparative analysis of PET and multiparametric MRI biomarkers in Alzheimer's disease continuum cohort

Journal of Alzheimer's
Disease Reports
Volume 9: 1–16
© The Author(s) 2025
Article reuse guidelines:
sagepub.com/journals-permissions
DOI: 10.1177/25424823251394399
journals.sagepub.com/home/alr



Chileka Chiyanika^{1,2}, Nga Yan Chan², Wanting Liu³, Lisa Wing Chi Au³, Weitian Chen², Chunlei Liu^{4,5}, Sirong Chen⁶, Eric Yim Lung Leung⁶, Chi Lai Ho⁶, Yuan Cai³, Ho Ko³, Qianyun Chen^{2,7}, Winnie Chu², Vincent Chung Tong Mok³ and Jill Abrigo²

Abstract

Background: Non-invasive biomarkers are key to early Alzheimer's disease (AD) detection. Multiparametric MRI and advanced imaging offer promising, accessible tools for identifying AD-related changes, supporting timely diagnosis and intervention.

Objective: To assess how accurately multiparametric MRI biomarkers identify AD using A β -PET imaging as the reference, and to evaluate whether MRI metrics in AD-related brain regions can distinguish between A β -positive and A β -negative subjects across the AD continuum.

Methods: In this exploratory retrospective study, 44 subjects aged 50–80 years were classified based on their PET and MRI biomarkers following the NIA-AA 2024 framework. MRI metrics included selected regional brain volumes (TI-weighted), mean diffusivity and fractional anisotropy (DTI-MD, DTI-FA), quantitative susceptibility mapping (QSM), and TIrho imaging. These were compared with amyloid load, and diagnostic performance was assessed using area-under-the-curve (AUC) analysis.

Results: 25 subjects were Aβ+ (AD continuum), while 19 were Aβ- (controls). Volumes of the hippocampus, thalamus, amygdala, cingulate, putamen, and corpus callosum and DTI-MD in the hippocampus, corpus callosum, cuneus, and cingulate showed optimal diagnostic performance (AUC \geq 0.80), with hippocampal volume and hippocampal DTI-MD showing AUCs > 0.90, (both p < 0.05). Combining hippocampal volumetry and hippocampal DTI-MD (AUC = 0.95, p < 0.001) improved diagnostic accuracy by 2.1% compared to using either biomarker alone. LASSO logistic regression analysis showed that amyloid positivity was significantly associated with hippocampal volume (p < 0.001).

Conclusions: Hippocampal volumetry and hippocampal DTI-MD may be superior and more sensitive imaging biomarkers for AD. Their combined use could improve diagnostic accuracy and enhance early AD detection.

Keywords

Alzheimer's disease, diffusion tensor imaging-fractional anisotropy, diffusion tensor imaging-mean diffusivity, quantitative susceptibility mapping, T1rho

Received: 16 June 2025; accepted: 19 October 2025

Corresponding author:

Jill Abrigo, Department of Imaging & Interventional Radiology, The Chinese University of Hong Kong, Prince of Wales Hospital, 30-32 Ngan Shing St, Shatin, Hong Kong SAR, China. Email: jillabrigo@cuhk.edu.hk

Creative Commons Non Commercial CC BY-NC: This article is distributed under the terms of the Creative Commons Attribution-NonCommercial 4.0 License (https://creativecommons.org/licenses/by-nc/4.0/) which permits non-commercial use, reproduction and distribution of the work without further permission provided the original work is attributed as specified on the SAGE and Open Access page (https://us.sagepub.com/en-us/nam/open-access-at-sage).

¹Department of Health Technology and Informatics, The Hong Kong Polytechnic University, Hong Kong, China

²Department of Imaging and Interventional Radiology, The Chinese University of Hong Kong, Prince of Wales Hospital, Hong Kong, China

³Gerald Choa Neuroscience Institute, Lui Che Woo Institute of Innovative Medicine, Lau Tat-Chuen Research Centre of Brain Degenerative Diseases Chinese, Division of Neurology, Department of Medicine and Therapeutics, The Chinese University of Hong Kong, Prince of Wales Hospital, Hong Kong, China

⁴Department of Electrical Engineering and Computer Sciences, University of California, Berkeley, CA, USA

⁵Helen Wills Neuroscience Institute, University of California, Berkeley, CA, USA

⁶Department of Nuclear Medicine & PET, Hong Kong Sanatorium & Hospital, Hong Kong, China

⁷Department of Radiology, Shenzhen Nanshan People's Hospital, Nanshan District, Shenzhen, China

Introduction

Alzheimer's disease (AD) is a progressive neurodegenerative disorder and the leading cause of dementia, recognized by the World Health Organization as a global healthcare priority. It affects one in nine individuals over 65 years and is the fifth leading cause of death worldwide. Currently, over 50 million people have dementia, with numbers expected to triple by 2050, particularly in lowand middle-income countries.

AD progresses through three primary stages: preclinical AD, mild cognitive impairment due to AD, and dementia related to AD.⁵ It is characterized by two main pathological features: extracellular amyloid- β (A β) plaques and intraneuronal neurofibrillary tangles (NFTs) composed of phosphorylated tau.⁶ These features develop years before clinical symptoms appear, with A β accumulation starting about 20 years and NFTs about 10 years before symptom onset.⁶ Therefore, AD is viewed as a continuum rather than three distinct clinical stages, with biomarkers reflecting this gradual progression.⁷

The key objective in diagnosing AD is to develop noninvasive biomarkers that can detect the disease early. These biomarkers should be sensitive, specific, clinically useful, and accessible, allowing for timely intervention and supporting precision medicine. Since the presence of Aß plagues is a strong indicator of AD, the framework from the National Institute on Aging and the Alzheimer's Association (NIA-AA) highlights the importance of positive amyloid biomarkers in identifying AD-related processes. However, AD is a complex and heterogeneous disorder, and recent advances have led to the adoption of the ATN (Amyloid, Tau, Neurodegeneration) framework and its expanded versions, such as ATN(IVS), for research and diagnosis.8 This multidimensional approach incorporates a broader spectrum of biomarkers including imaging and fluid markers of amyloid deposition (A), tau pathology (T), and neurodegeneration (N), as well as markers of inflammation/immune mechanisms (I), vascular brain injury (V), and synucleinopathy (S).8 Integrating these diverse biomarkers enhances diagnostic accuracy, enables earlier detection, and provides a more comprehensive understanding of disease progression. Thus, expanding the diagnostic focus beyond amyloid to include additional relevant biomarkers is crucial for the development of robust diagnostic tools and the implementation of effective prevention and treatment strategies.

Definitive confirmation of $A\beta$ and tau is through postmortem, which limits clinical-histological correlation during life. Therefore, in vivo methods like positron emission tomography (PET), magnetic resonance imaging (MRI), bloodbased biomarkers, and cerebrospinal fluid analysis have been developed to facilitate early and accurate clinical diagnosis of AD and aid potential therapeutic intervention. PET is the most established technique for visualizing $A\beta$ and tau

in vivo, but it has limitations, such as limited availability of radioactive tracers, high costs, 10 the short half-life of the ¹¹C isotope, ¹¹ and the tendency of Pittsburgh Compound B (PIB) to bind only to fibrillar forms of A_B. ¹² Alternative neuroimaging biomarkers have been developed to provide additional insights. T1 weighted structural MRI is commonly used to measure the volume of the hippocampus and other brain regions, enabling the assessment of regional brain atrophy in AD, while advanced MRI techniques like diffusion tensor imaging (DTI), quantitative susceptibility mapping (QSM), and T1rho offer additional insights into microstructural, biochemical, and pathological changes. DTI detects microstructural changes in white matter, which may be associated with AB and tau deposition among other pathological processes, as indicated by lower fractional anisotropy and higher mean diffusivity in affected areas. 13 This makes DTI a valuable tool for sensitively identifying early axonal degeneration and demyelination, which are characteristic features of AD. OSM assesses magnetic susceptibility to identify abnormal iron deposition and changes in myelination, hallmark features of AD, as well as to detect microbleeds, differentiate tissue types, monitor disease progression, and provide complementary information for improved diagnostic accuracy. 14 By quantifying brain iron accumulation and other susceptibility changes, QSM offers important insights into neurodegeneration and amyloid pathology in AD. T1rho is sensitive to pH changes, slow molecular motions, proteoglycan content, and chemical exchange processes that may be associated with Aβ and tau presence, making it effective in detecting both biochemical and structural changes. 15 Its ability to capture early alterations in the brain's macromolecular environment and tissue microstructure further supports its use as a potential biomarker for AD. 16 Together, these MRI sequences provide complementary and comprehensive information on the structural, biochemical, and pathological changes associated with AD, enhancing the detection and monitoring of the disease. Each method examines specific features of AD pathology, but no study has directly compared their diagnostic performance. Thus, this study aims to determine how accurately multiparametric MRI-based neuroimaging biomarkers can identify AD using Aβ-PET imaging as the reference standard. Specifically, we evaluate the ability of MRI-derived metrics (T1 weighted, MD, FA, QSM and T1rho) in different brain regions to distinguish between amyloid-positive and amyloid-negative subjects across the AD continuum.

Methods

Subjects

This study is an exploratory retrospective analysis based on data from the ongoing Chinese University of Hong Kong—Screening for Early Alzheimer's Disease Study (CU-SEEDS), which aims to identify imaging biomarkers for the early diagnosis of AD. Subjects were recruited

according to specific criteria: they had to be of Chinese ethnicity, aged between 50 and 80 years, and have Cantonese as their primary language. Subjects were excluded if they had a diagnosis of non-Alzheimer's dementia, a history of stroke, parkinsonism, major psychiatric illness, other significant neurological diseases (such as brain tumors), or any contraindications to MRI /PET imaging. Informed consent was obtained from all subjects. For the current analysis, we included Chinese men and women aged 50-80 years, without any diagnosed neurological disorders, who underwent both PET/CT and MRI scans. The MRI protocol included DTI (both MD and FA), T1-weighted imaging, OSM, and T1 rho imaging. Additional data collected included age, sex, years of education, cognitive impairment status (assessed using the Hong Kong List Learning Test), and Montreal Cognitive Assessment (MoCA) scores (Hong Kong version). The study was conducted in accordance with Helsinki declaration, and it was approved by the Ethics Committee of the Joint Chinese University of Hong Kong—New Territories East Cluster Clinical Research Ethics Committee (REF NO. 2017.254). Forty-four (44) subjects were analyzed after excluding thirty-four (34) subjects whose amyloid-PET results indicated non-Alzheimer's pathological changes according to the NIA-AA 2018 framework (I.e., A-T+N-, A-T-N+, A-T+N+). According to the ATN framework, Aβ+ (positive amyloid-beta) biomarker status is considered to be on the AD continuum, regardless of tau or neurodegeneration status or cognitive impairment. Therefore, our final sample comprised subjects with the following biomarker profiles: A-T-N- (normal AD biomarkers as controls), A + T - N - (Alzheimer's pathological change), A + T + N -, and A + T + N + (Alzheimer's disease).

Clinical staging of cognitive decline

Clinical staging was divided into four groups: normal control (NC), subjective cognitive decline (SCD), mild cognitive impairment (MCI), mild dementia (MD) and moderate to severe dementia (MSD):

- (i) Normal control (NC) was defined as subjects without subjective memory complaints, as indicated by an Abbreviated Memory Inventory for Chinese (AMIC) score < 1 (range: 0–5, with higher scores indicating worse memory)¹⁷ or an AD8[®] Dementia Screening Interview (AD8) score < 1 (range: 0–8, with higher scores indicating greater perceived change).¹⁸ They also did not have objective cognitive impairment, as demonstrated by a Hong Kong List Learning Test (HKLLT-T4) score > -1.0 standard deviation (SD) or a MoCA score > 16th percentile.
- (ii) SCD was defined as subjects with reported subjective memory complaints (AMIC or AD8 score ≥ 1) but did not show objective cognitive impairment.

- (iii) MCI was defined as subjects with SCD and objective cognitive impairment (HKLLT-T4 \leq -1.0 SD or MoCA \leq 16th percentile) but remained independent in performing daily tasks.
- (iv) Dementia (MD and MSD)- A senior neurologist diagnosed dementia and classified its severity as mild, moderate, or severe. This classification was based on the NIA-AA criteria¹⁹ and the Clinical Dementia Rating (CDR) score.²⁰

Given the limited number of subjects in some of the individual groups, in the analysis, we merged the SCD and MCI groups to form the 'early cognitive impairment' group and combined the MD and MSD groups to form the 'mild/moderate to severe dementia' group.

PET imaging

PET imaging was performed using a PET/CT scanner (BiographTM 16 LSO HI-REZ; CTI/Siemens Inc.) to quantify amyloid-beta, tau deposition, and glucose hypometabolism with ¹¹C-PIB, ¹⁸F-T807, and ¹⁸F-FDG, respectively. All subjects received ¹¹C-PIB intravenously and were scanned at 35 min post-injection. Within one week, ¹⁸F-T807 PET/CT was performed at 85 min post-injection. Data acquisition began with a non-contrast CT scan (130 kV, 110–115 mA, 2 mm pitch, 1 s tube rotation), followed by PET imaging with 81 axial planes and an axial field of view of 16.2 cm. PET and CT images were reconstructed using the ordered-subset expectation maximization (OSEM) algorithm (16 subsets, 8 iterations), with a 256×256 matrix for PET and a 512×512 matrix for CT.

All PET images were processed using a standardized pipeline as described in the image processing and registration section. Quantification of amyloid PET, tau PET, and FDG-PET was achieved using standardized uptake value ratios (SUVRs), with the cerebellar cortex serving as the reference region. SUVRs for each region-of-interest (ROI) were calculated by dividing the mean uptake in the ROI by the mean uptake in the cerebellar cortex. In the case of FDG-PET, mean FDG uptake was extracted from predefined ROIs segmented using FreeSurfer version 7. All co-registrations and segmentations were visually inspected for accuracy, and any misalignments were manually corrected.

The primary analysis exclusively focused on amyloid-beta PET data by quantifying ¹¹C-PIB uptake quantified using the global cortical to cerebellum standardized uptake value ratio (SUVR),²¹ calculated for each ROI as described in the image processing and registration section. These ROIs encompass key cortical regions commonly affected in amnestic AD. Tau-PET and FDG-PET data were used to categorize subjects according to the ATN (Amyloid/Tau/Neurodegeneration) framework.

MRI

All MRI scans were conducted using a 3 T scanner (Philips Achieva TX, Best, The Netherlands) equipped with an eight-channel head coil.

Structural MRI imaging and analysis

A 3D T1-weighted volumetric sequence was used to acquire the structural MRI image for calculation of ROI volumes and co-registration purposes. Parameters were set as follows: echo time (TE) of 3.5 ms, repetition time (TR) of 7.5 ms, flip angle of 8° , field of view of $250 \times 250 \times 171$ mm³, acquired resolution of $1.1 \times 1.1 \times 1.2$ mm³, and a SENSE acceleration factor of 2. ROI volume (ROI-V) and estimated total intracranial volume (eTIV) were obtained from FreeSurfer output. ROI-V was adjusted for eTIV using the formula²²: *Adjusted ROI-V* = raw ROI-V - b (eTIV - mean eTIV), where b represents the regression coefficient from regressing ROI-V against eTIV.

DTI (MD and FA) MRI imaging and processing

Axial diffusion MRI data were collected using 48 diffusion-encoding directions at a b-value of 1000 s/mm², along with six non-diffusion-weighted b0 images. The scanning parameters were as follows: TR of 8944 ms, TE of 60 ms, a flip angle of 90°, reconstructed voxel of 1 mm × 1 mm × 1 mm. The DTI scans were pre-processed using the FSL diffusion toolbox (Version 5.0.9, FMRIB, Oxford, UK, http://www.fmrib.ox.ac.uk/fsl/). First, the images were corrected for eddy currents and head motion using the FSL diffusion toolbox. Skull stripping was performed with the Brain Extraction Tool. The DTIfit tool was then used to fit diffusion tensors at each voxel and generate mean diffusivity (MD) and fractional anisotropy (FA) maps. These DTI maps were aligned to the individual T1-weighted anatomical images and standardized to the MNI reference coordinate system using deformation fields from T1 normalization. White matter masks and tractspecific ROIs (cingulum, fornix, and uncinate fasciculus) were derived using the FSL diffusion toolbox. The quality of normalization was visually inspected, and scan homogeneity was assessed by calculating the standard deviation across the sample. DTI maps were smoothed with an 8 mm Gaussian kernel to enhance signal-to-noise ratio, compensate for anatomical variability, and optimize statistical validity while preserving spatial resolution. Median FA and MD values were calculated within each ROI for each subject.

QSM MRI imaging and processing

Gradient-echo phase images were obtained using an eightecho 3D fast-field echo sequence for QSM analysis. The imaging parameters included a TE of 4.0 ms with a Δ TE of 5.2 ms, a TR of 45 ms, a flip angle of 20 degrees, an FOV of $40 \times 240 \times 120$ mm, an acquired resolution of $0.6 \times 0.8 \times 2$ mm, and a sensitivity encoding (SENSE) acceleration factor of 2.5. QSM raw phase images were first unwrapped using a Laplacian-based algorithm. Then, the background phase was removed using the variable spherical kernel size (V-SHARP) method. Finally, the susceptibility maps were generated using the streaking artifact reduction for QSM (STAR-QSM) technique available in the STI-Suite.

T1rho MRI imaging and processing

T1rho images were obtained with the following parameters: TR/TE of 2000 ms/12 ms, total spin lock (TSL) durations of 10, 20, 30, and 40 ms, a spin lock pulse amplitude of 500 Hz, a slice thickness of 2 mm, a field of view (FOV) of 24×24 cm², a matrix size of 256×128 , a bandwidth of 130 Hz per pixel, and an echo train length of 4. To eliminate the contribution of cerebrospinal fluid (CSF) to the T1rho-weighted MR signal, an inversion time (TI) of 860 ms was used, as described by Borthakur et al. ¹⁶ Voxel wise T1rho values and ROI averages were calculated using in-house MATLAB functions based on the following formula ²⁶: $M(TSL) = M_0 e^{-TSL/T_{1rho}}$. Where M(TSL) is the signal intensity at a given spin-lock time (TSL), M₀ is the initial signal intensity, and T₁rho is the spin-lattice relaxation time in the rotating frame.

Image processing and registration

For all imaging modalities, DICOM images were converted to NIFTI format using dcm2niix.²⁷ PET, QSM, and T1rho images were co-registered to individual T1-weighted images using the affine registration tool in Advanced Normalization Tools (ANTs), with skull stripping performed on T1²⁸ and CT²⁹ images to improve registration accuracy. ROIs for PET, QSM, T1rho, and structural MRI were automatically extracted, segmented and processed using FreeSurfer version 7. 30,31 Subcortical ROIs, including the hippocampus, were defined using the MNI (Montreal Neurological Institute) Structural Atlas, while cortical parcellation was performed with the Destrieux Atlas. 30 The following ROIs (Figure 1) were included across all imaging biomarkers: hippocampus, amygdala, thalamus, caudate, putamen, corpus callosum, cuneus and cingulate.³² Additional ROIs analyzed were: global cortex, precuneus, posterior cingulate cortex, and cerebellum for PET; globus pallidus for QSM and T1rho; cingulum for DTI; and total intracranial volume and cortical regions for structural MRI. Due to limited z-coverage, QSM and T1rho sequences did not include the cuneus and cingulate gyrus.

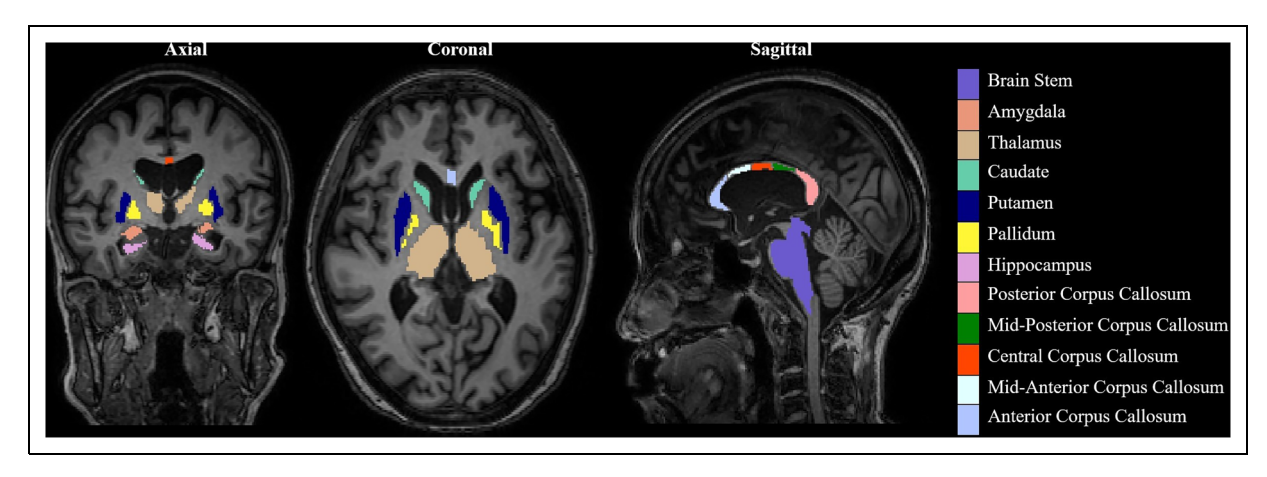


Figure 1. Illustrates the regions of interest in this study, as determined by MNI (Montreal Neurological Institute) Atlas, and shown in axial, coronal and sagittal views with a color scheme. The regions include: brain stem (purple)- vital for basic life functions; amygdala (peach)- involved in emotion regulation and memory; thalamus (tan)- acts as a relay station for sensory information; caudate (teal)-associated with motor processes and learning; putamen (dark blue)- plays a role in movement and learning; pallidum (yellow)- involved in the regulation of voluntary movement; hippocampus (pink)- critical for memory formation; corpus callosum (light pink/light blue/green/orange/red)- facilitates communication between the two hemispheres, integrates functions, coordinates motor activities, and supports cognitive processing.

Quality control procedures

Rigorous quality control (OC) procedures were implemented to ensure the accuracy and reliability of brain imaging data in this study. Following image acquisition and preprocessing steps, including registration, QC was conducted using both automated and manual approaches. Visual inspection was routinely performed by overlaying registered images onto standard templates and examining them slice-by-slice to verify proper alignment of anatomical structures and to identify any artifacts or misregistration. In addition, automated quality metrics, such as similarity indices and deformation field analyses, were utilized to quantitatively assess registration accuracy and detect outliers. Standardized QC checklists and protocols were employed to maintain consistency across raters and sessions, and specialized software tools were used to flag images with potential quality issues. Images failing to meet quality standards were either reprocessed or excluded from further analysis. All QC steps and decisions were thoroughly documented to ensure transparency and reproducibility, thereby enhancing the validity of the study findings.

AD definition based on imaging biomarkers

The NIA-AA 2024 framework proposed that amyloid- β (A) PET positivity alone is a core diagnostic criterion for AD, while tau (T) PET and neurodegeneration (N) are markers for staging and monitoring disease progression.³³ In this study, the ATN classification was used solely for inclusion and exclusion criteria: each biomarker was classified as positive (+) or negative (–), and subjects were categorized based on the presence or absence of A β .

Aβ+ was defined as an abnormal uptake in ¹¹C-Pittsburgh compound B (PIB), visually identified and/ or with an SUVR $\geq 1.42^{32}$ in the specified ROIs.^{34,35} T+was defined as an abnormal uptake in ¹⁸F-flortaucipir (¹⁸F-T807), visually identified and/or with SUVR >1.23³² in the relevant ROIs. N+was defined as abnormal glucose metabolism of 18-Fludeoxyglucose (F18-FDG) PET with weighted median SUVR ≥ 1.21. 36 These SUVR thresholds were selected based on established values reported in the literature. 32,36 Such thresholds are widely used in both research and clinical practice to distinguish biomarker positivity. All PET scans were independently reviewed by a nuclear medicine specialist with over 20 years of experience, blinded to the subjects' cognitive data. Importantly, only Aβ-PET was used for group analyses in this study; tau and neurodegeneration data were collected exclusively for subject classification according to the NIA-AA 2018 framework and were not included in the main analyses.

Statistical analysis

The data were not normally distributed, as indicated by skewness and kurtosis assessments. Therefore, continuous variables were reported as median (range) to accurately represent central tendency and variability without the influence of outliers, unless stated otherwise. Averages were used to compute data from various ROIs within the same anatomical structure and/or from paired structures. Of note, analysis of absolute QSM values was performed to provide a single metric for the total magnitude of susceptibility change, capturing both paramagnetic (e.g., iron accumulation) and diamagnetic (e.g., demyelination) effects.

Variable	Aβ- (n = 19)	$A\beta + (n = 25)$	Р	
Age (y)	64 (52–72)	70 (50–79)	0.007#	
Sex: female/male, n (%)	10/9 (52.6/47.2)	18/7 (72/28)	0.191*	
NC, n (%)	3 (15.8)	I (4)	0.183*	
SCD, n (%)	16 (84.2)	3 (12)	<0.001*	
MCI, n (%)	0	14 (56)	<0.001*	
MD, n (%)	0 (0)	6 (24)	0.023*	
MSD, n (%)	0 (0)	l (4)	0.383*	
Education (y)	11(5–21)	9 (0–17)	0.517#	
MoCA score	28 (26–30)	19 (4–30)	<0.001#	
HKLLT z-score	0.41 (-0.9788)	-2.03(-3-2)	<0.001#	
A-T-N-, n (%)	19 (100)	0 (0)	<0.001*	
A + T + N -, n (%)	0 (0)	16 (64)		
A + T + N+, n (%)	0 (0)	9 (36)		
A + T-N-, n (%)	0 (0)	0 (0)	1.000	
A + T-N+, n (%)	0 (0)	0 (0)	1.000	

Table 1. Demographic, clinical staging of cognitive impairment and positron emission tomography characteristics of the subjects.

#Mann-Whitney test was used. *Fisher's exact test was used. Values are expressed as median (range) unless stated otherwise. Aβ: amyloid-β; AD: Alzheimer's disease; NC: normal control; SCD: subjective memory decline; MCI: mild cognitive impairment; MD: mild dementia; MSD: moderate to severe dementia; MoCA: Montreal Cognitive Assessment score; HKLLT: Hong Kong List Learning Test. A-T-N-: normal AD biomarkers; A + T-N-: Alzheimer's pathological change; A + T + N- and A + T + N+: Alzheimer's disease; A + T-N+: Alzheimer's and concomitant suspected non-Alzheimer's pathologic change. Statistically significant (p < 0.05).

This approach prevents these competing signals from canceling each other out, thereby revealing important underlying pathology and providing a more complete picture of the disease. Categorical variables were shown as counts with corresponding percentages. For comparisons between two groups, the Mann-Whitney test was used for continuous data, and Fisher's exact test was used for categorical data.

The diagnostic performance of each variable was assessed using the area under receiver operating characteristic curves (AUC) to distinguish between Aβ+ and Aβsubjects. Pairwise comparisons of AUC values for different MRI metrics were conducted using the DeLong test. AUC values were interpreted as follows³⁷: 0.90-1.00 as excellent, 0.80-0.89 as good, 0.70-0.79 as fair, 0.60-0.69 as poor, and 0.50-0.59 as fail. Post hoc analysis was performed to assess whether combining the two best predictors of A\beta+ would enhance the diagnostic performance of the imaging biomarkers. To achieve this, three models were constructed from the two predictors: each predictor was evaluated individually as a model, and then both were combined in a third model. Logistic regression was performed to obtain the probabilities for each model. Predicted probabilities were used to generate ROC curves, with optimal classification thresholds determined by Youden's index. Sensitivity, specificity, accuracy, positive predictive value, negative predictive value, and AUC were calculated for each model. Model performance was compared using DeLong's test for correlated AUCs, with 95% confidence intervals and p-values reported for differences in AUC.

To identify key predictors of $A\beta+$, LASSO (Least Absolute Shrinkage and Selection Operator) logistic regression was performed using age, sex, education, and a comprehensive set of neuroimaging biomarkers as predictors.

LASSO regression was implemented with cross-validation to select the optimal regularization parameter, allowing for simultaneous variable selection and regularization to prevent overfitting in the context of high-dimensional data. The dependent variable was A β + (AD continuum), a binary outcome. To assess the stability and significance of the selected predictors, bootstrapping with 1000 resamples was performed to estimate mean coefficients and 95% confidence intervals for each variable. Model performance was evaluated using accuracy and the AUC. All statistical tests were two-sided, and p-values less than 0.05 were considered statistically significant. Analyses were performed using SPSS (version 28.0, IBM, Chicago, IL), MedCalc (version 23.0.6) and Python (version 3.13).

Results

Demographic and clinical characteristics

Of the 78 subjects screened for AD, 44 were included in the final analysis: 19 controls (A β -) and 25 on the AD continuum (A β +). The median age was significantly higher in the A β + group (70 years, range 50–79 years) compared to the A β - group (64 years, range 52–72 years; p=0.007). Cognitive performance, as measured by MoCA and HKLLT z-scores, was significantly lower in the A β + group (both p<0.001). Detailed demographic and clinical characteristics are presented in Table 1.

Regional imaging outcomes

Compared to the A β - group, the A β + group exhibited significantly higher global amyloid deposition (p<0.001)

Table 2. Multimodal and multiparametric regional imaging outcomes between A β - and A β + patients.

Variable	A β - (n = 19)	$A\beta + (n = 25)$	Р
Global amyloid deposition (SUVR)	1.09 (0.90–1.22)	1.51 (0.78–2.18)	<0.001
Global tau deposition (SUVR)	1.33 (1.05–1.71)	1.38 (1.02–2.41)	0.166
Adjusted Thalamus volume (ml)	6.81 (5.71–7.53)	6.01(4.25–6.74)	<0.001
Adjusted Caudate volume (ml)	3.33 (2.65–4.12)	3.09 (2.34–3.87)	0.051
Adjusted Putamen volume (ml)	5.04 (3.79–5.79)	4.18 (3.54–4.99)	<0.001
Adjusted Hippocampal volume (ml)	8.12 (7.59–9.92)	5.96 (4.59–8.06)	<0.001
Adjusted Amygdala volume (ml)	1.81 (1.48–2.30)	1.32 (0.78–1.80)	<0.001
Adjusted Corpus callosum volume (ml)	3.29 (2.77–3.93)	2.91 (2.19–3.79)	<0.001
Adjusted Cuneus volume (ml)	3.75 (2.98–4.51)	3.53 (2.95–4.97)	0.166
Adjusted Cingulate volume (ml)	10.34 (9.01–12.33)	9.03 (7.47–12.09)	<0.001
DTI-MD Thalamus (mm ² /s)	0.0009 (0.0085-0.0013)	0.0011 (0.0009-0.002)	0.038
DTI-MD Caudate (mm ² /s)	0.0010 (0.0089–0.002)	0.0011 (0.0009–0.002)	0.087
DTI-MD Putamen (mm ² /s)	0.00070 (0.0006–0.0008)	0.00072 (0.00065–0.0008)	0.096
DTI-MD Hippocampus (mm ² /s)	0.0010 (0.0091–0.0012)	0.0012 (0.00099–0.00165)	<0.001
DTI-MD Amygdala (mm ² /s)	0.00081 (0.0067–0.00104)	0.00083 (0.00077–0.00116)	0.038
DTI-MD Corpus callosum (mm²/s)	0.00104 (0.0010-0.00164)	0.00133 (0.00108–0.00208)	<0.001
DTI-MD Cuneus (mm ² /s)	0.00113 (0.0095–0.00137)	0.00134 (0.0099–0.00167)	<0.001
DTI-MD Cingulate (mm ² /s)	0.0009 (0.00089–0.0012)	0.00111 (0.00095–0.00131)	<0.001
DTI-FA Thalamus (mm²/s)	0.33 (0.28–0.36)	0.31 (0.24–0.36)	0.107
DTI-FA Caudate (mm ² /s)	0.21 (0.19–0.32)	0.22 (0.18–0.31)	0.478
DTI-FA Putamen (mm²/s)	0.31 (0.25–0.37)	0.32 (0.28–0.42)	0.149
DTI-FA Hippocampus (mm²/s)	0.202 (0.167–0.320)	0.172 (0.134–0.312)	0.002
DTI-FA Amygdala (mm ² /s)	0.239 (0.217–0.272)	0.226 (0.196–0.303)	0.007
DTI-FA Corpus callosum (mm²/s)	0.47 (0.27–0.60)	0.47 (0.13–0.54)	0.118
DTI-FA Cuneus (mm²/s)	0.15 (0.12–0.20)	0.14 (0.10-0.21)	0.678
DTI-FA Cingulate (mm ² /s)	0.194 (0.17–0.22)	0.187 (0.17–0.22)	0.096
QSM Thalamus (ppm)	0.00207 (0.0001–0.0045)	0.00376 (0.0001–0.0102)	0.039
QSM Caudate (ppm)	0.0288 (0.0138–0.0352)	0.0323 (0.0214–0.0505)	0.111
QSM Putamen (ppm)	0.0177 (0.006–0.0327)	0.0233 (0.0172–0.0521)	0.010
QSM Hippocampus (ppm)	0.0026 (0.00005–0.00579)	0.0025 (0.000008–0.00599)	0.937
QSM Amygdala (ppm)	0.00115 (0.0001–0.00566)	0.00262 (0.00025–0.0110)	0.388
QSM Corpus callosum (ppm)	0.00539 (0.0001–0.0174)	0.00527 (0.00022–0.0242)	0.676
TIrho Thalamus (ms)	78.25 (74.66–84.54) ´	77.58 (60.14–88.33)	0.271
TIrho Caudate (ms)	77.41 (72.14–84.34)	77.54 (66.39–82.85)	0.271
TIrho Putamen (ms)	74.98 (66.53–83.30)	75.29 (63.86–80.48)	0.387
TIrho Hippocampus (ms)	84.69 (79.70–100.2 ¹)	81.82 (75.02–97.11)	0.005
TIrho Amygdala (ms)	80.73 (75.59–95.16) [´]	79.53 (73.86–83.20)	0.485
TIrho Corpus callosum (ms)	78.21 (73.11–85.51)	77.46 (64.44–88.78)	0.325

Mann-Whitney test was used. Values are expressed as median (range). AD: Alzheimer's disease; Amyloid deposition as reflected by 11C-Pittsburgh compound B tracer retention; Tau deposition as reflected by ¹⁸F-flortaucipir retention; SUVR: standardized uptake value ratio; T1rho: Time constant of spin-lattice relaxation in rotating frame; QSM: Quantitative Susceptibility mapping; DTI-MD: Diffusion tensor imaging-mean diffusivity; DTI FA: Diffusion tensor imaging- fractional anisotropy; ms: milliseconds; ppm: part per million; ml: milliliter: Significant level, p < 0.05. Corpus Callosum included the following regions: Posterior, Mid Posterior, Central, Mid Anterior, and Anterior. Cingulate included these regions in both the left and right sides: Caudal Anterior, Posterior, Rostral Anterior, and Isthmus.

and significantly lower volumes in the hippocampus (p < 0.001), thalamus (p < 0.001), putamen (p < 0.001), amygdala (p < 0.001), corpus callosum (p < 0.001), cuneus (p < 0.001), and cingulate (p < 0.001). The caudate volume was also lower in the A β + group, but this difference was only marginally significant (p = 0.051). DTI-MD values were significantly elevated in the thalamus (p = 0.038), hippocampus (p < 0.001), amygdala (p = 0.038), corpus callosum (p < 0.001), cuneus (p < 0.001), and cingulate (p < 0.001). DTI-FA was significantly reduced in the hippocampus (p = 0.002) and amygdala (p = 0.007). QSM values were higher in the thalamus (p = 0.039) and putamen (p =

0.010), while T1rho was lower in the hippocampus (p = 0.005). Full regional imaging outcomes are provided in Table 2 and Figure 2.

Discriminative performance of neuroimaging biomarkers

Several imaging biomarkers demonstrated strong ability to distinguish between A β - and A β + groups as follows: Hippocampal volume (AUC = 0.94, p < 0.001), Thalamus volume (AUC = 0.90, p < 0.001), Amygdala volume

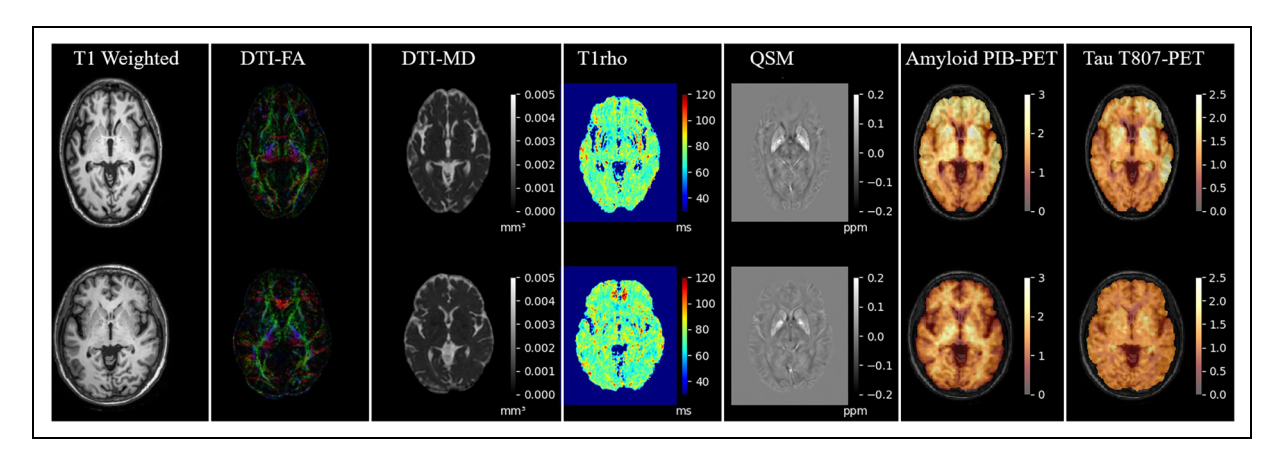


Figure 2. Images from two representative subjects. Top row shows a 70-year-old female subject with Alzheimer's disease (A+T+N+). Her Montreal Cognitive Assessment score was 16/30, Hong Kong List Learning Test z score of -2.24, 4 years of education and cognitively impaired. The bottom row displays a 72-year-old female subject without Alzheimer's disease (A-T-N-). Her Montreal Cognitive Assessment score was 28/30, Hong Kong List Learning Test z score of 1.26, 11 years of education and cognitively unimpaired. The brain images were obtained from: T1 weighted MRI, Diffusion tensor imaging-Fractional anisotropy (DTI-FA), Diffusion tensor imaging-mean diffusivity (DTI-MD), T1 rho, Quantitative susceptibility mapping (QSM), amyloid positron emission tomography (PET) and tau (PET).

(AUC = 0.90, p < 0.001), Cingulate volume (AUC = 0.84, p < 0.001), Putamen volume (AUC = 0.80, p < 0.001), Corpus callosum volume (AUC = 0.80, p < 0.001), DTI-MD in the hippocampus (AUC = 0.92, p < 0.001), corpus callosum (AUC = 0.84, p < 0.001), cuneus (AUC = 0.83, p < 0.001), and cingulate (AUC = 0.83, p < 0.001). DTI-FA in the hippocampus (AUC = 0.76, p = 0.003), amygdala (AUC = 0.73, p = 0.003), T1rho in the hippocampus (AUC = 0.75, p = 0.001), and QSM in the thalamus (AUC = 0.71, p = 0.001). Other regions and biomarkers had AUC values between 0.60–0.69 and 0.50–0.59 (all p > 0.05), indicating poor discrimination. Supplemental Table 1 provides further details.

Post hoc analysis of the best two performing neuroimaging biomarkers

Hippocampal volumetry and DTI-MD in the hippocampus were identified as the best performing biomarkers for distinguishing between A β - and A β + groups. The combination of both hippocampal volume and DTI-MD in the hippocampus achieved (AUC = 0.95, p < 0.001) but was not significantly different to that of hippocampal volume alone (AUC = 0.94, p = 0.334) and DTI-MD in the hippocampus alone (AUC = 0.92, p = 0.137). Details are shown in Supplemental Table 2.

Pairwise comparative analysis of multiparametric neuroimaging biomarkers in regions that were significantly different between $A\beta$ - and $A\beta$ + groups

Pairwise comparisons using the DeLong test were conducted to directly compare the diagnostic performance of

imaging biomarkers within the same brain region (ROI). In the hippocampus, hippocampal volume (AUC = 0.94) outperformed DTI-FA (AUC = 0.76, p = 0.013), QSM (AUC = 0.54, p < 0.001), and T1rho (AUC = 0.75, p =0.018), but was not significantly different from DTI-MD (AUC = 0.92, p = 0.499). In the corpus callosum, DTI-MD (AUC = 0.84) was superior to DTI-FA (AUC = 0.62, p=0.004) and QSM (AUC=0.56, p=0.017). In the thalamus, thalamus volume (AUC = 0.90) was superior to DTI-MD (AUC = 0.67, p = 0.033), DTI-FA (AUC = 0.65, p = 0.009), QSM (AUC = 0.71, p = 0.007) and T1rho (AUC = 0.62, p = 0.001). In the amygdala, amygdala volume (AUC = 0.90) was superior to DTI-MD (AUC = 0.66, p = 0.012), QSM (AUC = 0.56, p = 0.002) and T1rho (AUC = 0.55, p = 0.002). In the putamen, putamen volume (AUC = 0.80) was superior to DTI-FA (AUC = 0.60, p=0.033). In the cuneus, DTI-MD (AUC=0.83) was significantly better than DTI-FA (AUC = 0.53, p = 0.004) and cuneus volume (AUC = 0.61, p = 0.006). No significant differences were observed in other regions. Detailed results are shown in Figure 3 and Supplemental Tables 3-9.

Neuroimaging biomarkers as predictors of $A\beta$ positivity

The LASSO regression model demonstrated excellent classification performance (accuracy = 93.3%, AUC = 0.94), indicating strong discrimination between subjects with A β - and A β +. A variable was deemed to have a statistically significant association with A β + if the 95% CI for its mean coefficient did not contain 0 and the 95% CI for its odds ratio did not contain 1. Based on these

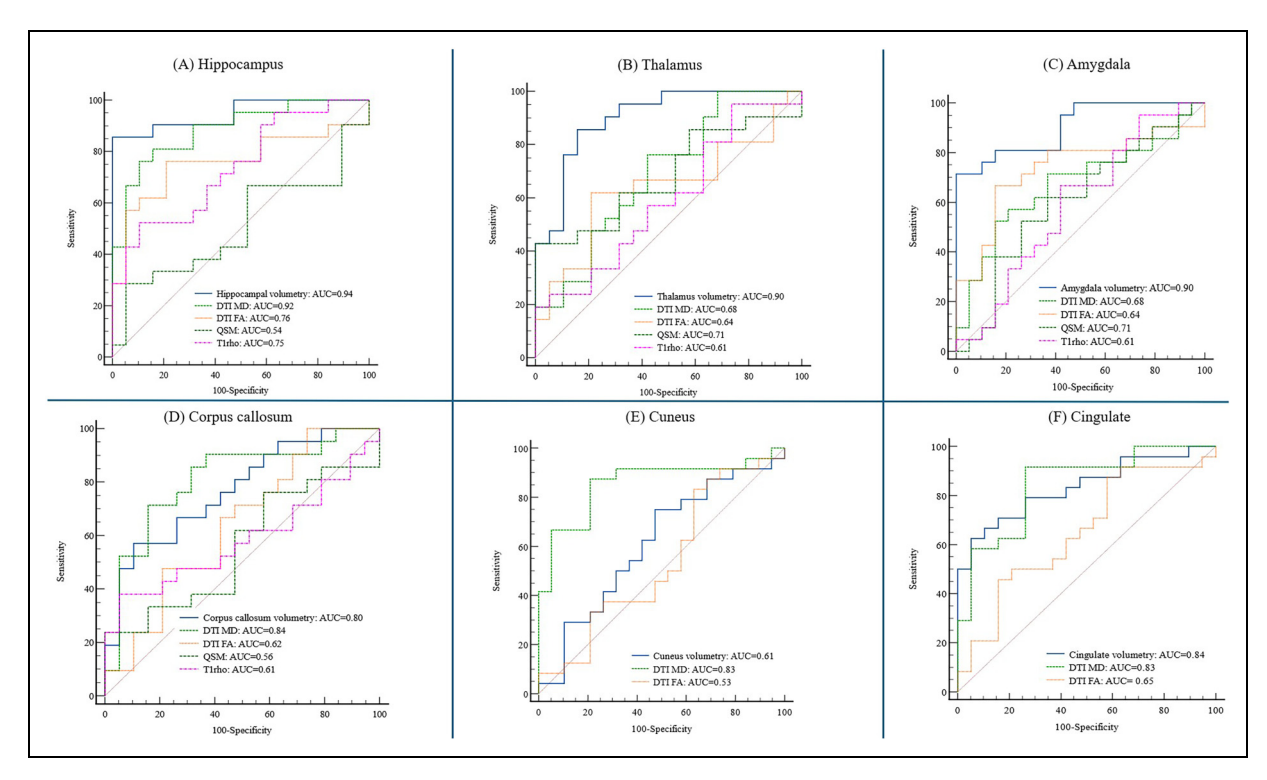


Figure 3. Shows the area under receiver characteristic operating curves (AUC) of various MRI biomarkers in regions that were significantly different between the Aβ- and Aβ+ subjects. T1 weighted: T1 weighted MRI for volumes in the hippocampus, thalamus, amygdala, corpus callosum, cuneus and cingulate; DTI-MD: diffusion tensor imaging- mean diffusivity; DTI-FA: diffusion tensor imaging- fractional anisotropy; QSM: quantitative susceptibility mapping; T1rho: T1 relaxation time in the rotating frame.

strict criteria, only hippocampal volume (mean coefficient: -2.43, 95% CI: -5.36 to -0.80) was a strong predictor, with an Odds Ratio (OR) of 0.005 (95% CI: 0.05 to 0.45), with both intervals excluding the null values. This indicates that a smaller or lower hippocampal volume was significantly associated with a higher likelihood of A β +.

The analysis also showed numerous variables with 'borderline significance', with their 95% CI for both the mean coefficient and the odds ratio touching the respective null value of 0 and 1, respectively. These included several brain region volumes (Thalamus, Putamen, Amygdala, Cingulate, Corpus callosum), T1rho measurements (Thalamus, Putamen, Hippocampus), QSM measurements (Caudate, Putamen, Hippocampus), DTI-MD measurements (Thalamus, Putamen, Hippocampus, Cuneus, Cingulate, Corpus callosum), and DTI-FA measurements (Thalamus, Putamen, Hippocampus, Amygdala, Cuneus, Corpus callosum). Detailed results are presented in Table 3.

Sub-analysis: Discrimination of early cognitive impairment and dementia severity

To distinguish between subjects with 'early cognitive impairment' from those with varying dementia severity

(mild/moderate to severe dementia) based solely on clinical classification, we performed a sub analysis. In the whole cohort, imaging biomarkers showed good discrimination between subjects with 'early cognitive impairment' (n = 37) and those with 'mild/moderate to severe dementia' (n=7). Thalamus and Amygdala volumes showed the strongest predictive power (both AUC = 0.90, p < 0.0001). Hippocampal volume and DTI-MD in the cuneus also performed well (both AUC = 0.89, p < 0.0001). Other variables that showed strong predictive capability included DTI-MD in the cingulate (AUC = 0.86, p < 0.0001), Cingulate volume (AUC = 0.84, p < 0.0001), DTI-MD in the amygdala (AUC = 0.81, p < 0.0001), Putamen volume (AUC = 0.80, p<0.0001), and Corpus callosum volume (AUC= 0.80, p < 0.0001). Other regions and biomarkers had AUC values between 0.70-0.79 and 0.50-0.59. Details are shown in Table 4.

Discussion

This study used a region of interest approach on selected cortical and subcortical regions relevant to AD based on previous literature. By successfully co-registering multimodal and multiparametric data, we were able to examine the relationships between amyloid deposition and MRI-based biomarkers, thereby providing a comprehensive characterization

Table 3. Bootstrapped mean LASSO regression analysis of imaging biomarkers and demographics for predicting amyloid-beta positivity.

Predictor	Mean coefficient	95% Confidence interval for mean coefficient			95% Confidence interval for ODD ratio	
		Lower	Upper	ODDS ratio	Lower	Upper
Age	0.01	-0.63	0.82	0.53	2.27	0.53
Sex	-0.05	-0.89	0.34	0.41	1.40	0.41
Education	-0.03	-0.79	0.42	0.45	1.52	0.45
Adjusted Thalamus volume	-0.14	-0.97	0.00	0.94	0.77	1.00
Adjusted Caudate volume	0.14	-0.02	0.86	1.00	1.00	1.00
Adjusted Putamen volume	-0.40	-1.60	0.00	0.89	0.70	1.00
Adjusted hippocampal volume	-2.43	-5.36	-0.80	0.005	0.45	0.005
Adjusted Amygdala volume	-0.28	-1.28	0.00	0.86	0.72	1.00
Adjusted Cuneus volume	0.09	-0.46	0.94	1.00	0.93	1.03
Adjusted Cingulate volume	-0.28	-1.13	0.00	0.87	0.72	1.00
Adjusted Corpus callosum volume	-0.52	-1.63	0.00	0.86	0.69	1.00
T I rho Thalamus	-0.30	-1.75	0.00	0.17	1.00	0.17
T1rho Caudate	-0.03	-0.49	0.07	0.61	1.07	0.61
T1rho Putamen	-0.44	-2.07	0.00	0.13	1.00	0.13
T1rho Hippocampus	-0.44	-1.91	0.00	0.15	1.00	0.15
T1rho Amygdala	0.15	-0.05	1.30	0.95	3.67	0.95
TIrho Corpus Callosum	-0.13	-1.30	0.06	0.27	1.06	0.27
OSM-Thalamus	0.06	-0.27	0.88	0.76	2.41	0.76
OSM-Caudate	-0.04	-0.60	0.00	0.55	1.00	0.55
OSM-Putamen	0.23	0.00	1.53	1.00	4.61	1.00
QSM-Hippocampus	0.31	0.00	1.91	1.00	6.76	1.00
QSM-Amygdala	0.01	-0.53	0.69	0.59	1.99	0.59
QSM-Corpus Callosum	-0.05	-0.78	0.06	0.46	1.06	0.46
DTI MD-Thalamus	0.02	0.00	0.24	1.00	1.27	1.00
DTI MD-Caudate	-0.03	-0.49	0.07	0.61	1.07	0.61
DTI MD-Putamen	0.29	0.00	1.51	1.00	4.53	1.00
DTI MD-Hippocampus	0.36	0.00	2.40	1.00	11.02	1.00
DTI MD-Amygdala	-0.02	-0.44	0.11	0.64	1.12	0.64
DTI MD-Cuneus	1.32	0.00	3.74	1.00	42.18	1.00
DTI MD-Cingulate	0.19	0.00	1.63	1.00	5.10	1.00
DTI MD-Corpus callosum	0.05	0.00	0.60	1.00	1.82	1.00
DTI FA-Thalamus	-0.08	-0.85	0.00	0.43	1.00	0.43
DTI FA-Caudate	-0.05 -0.15	-0.65 -1.46	0.17	0.43	1.19	0.43
DTI FA-Putamen	-0.13 -0.01	-0.15	0.17	0.23	1.17	0.23
DTI FA-Hippocampus	-0.01 -0.12	-0.13 -1.35	0.00	0.26	1.00	0.86
DTI FA-Hippocampus DTI FA-Amygdala	-0.12 -0.77	-1.33 -2.84	0.00	0.26	1.00	0.26
DTI FA-Amygdala DTI FA-cuneus	-0.77 -0.04	-2.6 4 -0.59	0.00	0.55	1.00	0.55
DTI FA-cuneus DTI FA- cingulate- Whole	-0.0 4 -0.08	-0.59 -1.02	0.00	0.36	1.00	0.36
	-0.08 -0.02	-0.29	0.23	0.36	1.26	0.36
DTI FA- Corpus Callosum	-0.02	-0.29	0.00	0.75	1.00	0.75

LASSO regression analysis was performed using Python. Significant; 95% CI does not include zero, Borderline; 95% CI just touches zero (lower or upper bound is zero), Not significant; 95% CI includes zero. TI rho; QSM: Quantitative susceptibility mapping; 0DTI-MD: Diffusion tensor imaging-mean diffusivity; DTI FA: Diffusion tensor imaging-fractional anisotropy. *QSM and TI rho were not performed in the cuneus and cingulate due to practical and technical difficulties in obtaining clear data. Corpus Callosum included the following regions: Posterior, Mid Posterior, Central, Mid Anterior, and Anterior. Cingulate included these regions in both the left and right sides: Caudal Anterior, Posterior, Rostral Anterior, and Isthmus.

of brain regions affected by AD. The subjects underwent amyloid and tau PET/CT, T1-weighted structural MRI for multiple regional volumetry, DTI-MD/DTI-FA, QSM and T1rho imaging. Subjects were categorized in two groups: an AD continuum group $(A\beta+)$ and a control group $(A\beta-)$.

The main findings of this study were as follows: (1) Significant differences were observed between subjects with $A\beta+$ and $A\beta-$ in several imaging biomarkers, including

volumes of the hippocampus, thalamus, putamen, amygdala, corpus callosum, and cingulate; DTI-MD in the thalamus, hippocampus, amygdala, corpus callosum, cuneus, and cingulate; DTI-FA in the hippocampus and amygdala; QSM in the thalamus and putamen; and T1rho in the hippocampus. (2) Lower hippocampal volume was significantly associated with a higher likelihood of A β +. (3) In differentiating between "early cognitive impairment" and "mild to

Table 4. Whole cohort multiparametric neuroimaging biomarkers for differentiating clinically diagnosed 'early cognitive impairment' and mild/moderate-severe dementia across brain regions.

MRI biomarker	AUC	SE	Youden index J	Sensitivity (%)	Specificity (%)	Р
Adjusted Thalamus volume	0.90 (0.78-0.97)	0.04	0.72	72 (50.6–87.9)	100 (82.4–100)	<0.0001
Adjusted Caudate volume	0.67 (0.52-0.81)	0.09	0.40	72 (50.6–87.9)	68 (43.4–87.4)	0.051
Adjusted Putamen volume	0.80 (0.66–0.91)	0.07	0.54	96 (79.6–99.9)	58 (33.5–79.7)	<0.0001
Adjusted Hippocampal volume	0.89 (0.75–0.96)	0.07	0.66	71.43 (29.0–96.3)	94.29 (80.8–99.3)	<0.0001
Adjusted Amygdala volume	0.90 (0.78-0.97)	0.04	0.72	72 (50.6–87.9)	100 (82.4–100)	<0.0001
Adjusted Corpus callosum volume	0.80 (0.65-0.90)	0.07	0.49	60 (38.7–78.9)	89 (66.9–98.7)	<0.0001
Adjusted cuneus volume	0.62 (0.46-0.77)	0.09	0.29	76 (54.9–90.6)	53 (28.9–75.6)	0.162
Adjusted Cingulate volume	0.84 (0.70-0.93)	0.06	0.59	64 (42.5–82.0)	95 (74.0–99.9)	<0.0001
DTI-MD Thalamus	0.64 (0.51-0.76)	0.11	0.36	64.81 (50.6–77.3)	71.43 (29.0–96.3)	0.197
DTI-MD Caudate	0.64 (0.51-0.76)	0.11	0.39	53.70 (39.6–67.4)	85.71 (42.1–99.6)	0.207
DTI-MD Putamen	0.50 (0.37-0.63)	0.16	0.25	96.30 (87.3–99.5)	28.57 (3.7–71.0)	0.993
DTI-MD Hippocampus	0.78 (0.63-0.90)	0.09	0.47	47.06 (29.8–64.9)	100.0 (59–100)	0.002
DTI-MD Amygdala	0.81 (0.66-0.92)	0.08	0.59	58.82 (40.4–75.4)	100 (59–100)	<0.0001
DTI-MD Corpus callosum	0.76 (0.60-0.88)	0.08	0.53	52.94 (35.1-70.2)	100 (59–100)	0.003
DTI-MD Cuneus	0.89 (0.75-0.97)	0.05	0.77	91.18 (76.3–98.1)	85.71 (42.1–99.6)	<0.0001
DTI-MD Cingulate-whole	0.86 (0.71-0.95)	0.07	0.62	76.47 (58.8–89.3)	85.71 (42.1–99.6)	<0.0001
DTI-FA Thalamus	0.64 (0.51-0.76)	0.15	0.40	83.33 (70.7–92.1)	57.14 (18.4–90.1)	0.330
DTI-FA Caudate	0.64 (0.51-0.76)	0.14	0.34	90.74 (79.7–96.9)	42.86 (9.9-81.6)	0.301
DTI-FA Putamen	0.68 (0.52-0.82)	0.14	0.43	100 (89.7–100)	42.86 (9.9-81.6)	0.185
DTI-FA Hippocampus	0.72 (0.56-0.85)	0.13	0.48	76.47 (58.8–89.3)	71.43 (29.0–96.3)	0.094
DTI-FA Amygdala	0.61 (0.48-0.74)	0.16	0.37	94.44 (84.6–98.8)	42.86 (9.9–81.6)	0.465
DTI-FA Corpus callosum	0.67 (0.53-0.78)	0.10	0.36	50 (36.1–63.9)	85.71 (42.1–99.6)	0.109
DTI-FA Cuneus	0.55 (0.42-0.68)	0.15	0.25	96.3 (87.3–99.5)	28.57 (3.7–71)	0.740
DTI-FA Cingulate-whole	0.66 (0.53-0.78)	0.13	0.38	66.67 (52.5–78.9)	71.43 (29.0–96.3)	0.208
QSM Thalamus	0.56 (0.42-0.69)	0.12	0.46	62.26 (47.9–75.2)	83.33 (35.9–99.6)	0.612
QSM Caudate	0.79 (0.63-0.91)	0.10	0.55	87.88 (71.8–96.6)	66.67 (22.3–95.7)	0.001
QSM Putamen	0.79 (0.63-0.91)	0.10	0.58	57.58 (39.2–74.5)	100 (54.1-100.0)	0.003
QSM Hippocampus	0.59 (0.45-0.72)	0.19	0.50	83.02 (70.2–91.9)	66.67 (22.3–95.7)	0.641
QSM Amygdala	0.52 (0.39-0.65)	0.13	0.21	54.72 (40.4–68.4)	66.67 (22.3–95.7)	0.886
QSM Corpus callosum	0.57 (0.43-0.70)	0.13	0.31	48.08 (34.0-62.4)	83.33 (35.9–99.6)	0.618
T1rho Thalamus	0.78 (0.63-0.89)	0.09	0.60	74.29 (56.7–87.5)	85.71 (42.1–99.6)	0.001
T1rho Caudate	0.64 (0.48-0.73)	0.12	0.30	87.27 (75.5–94.7)	42.86 (9.9–81.6)	0.383
T1rho Putamen	0.54 (0.41–0.67)	0.12	0.20	34.55 (22.2–48.6)	85.71 (42.199.6)	0.726
T1rho Hippocampus	0.76 (0.61–0.88)	0.10	0.49	77.14 (59.9–89.6)	71.43 (29.0–96.3)	0.01
T1rho Amygdala	0.56 (0.43-0.69)	0.10	0.26	54.55 (40.6–68.0)	71.43 (29.0–96.3)	0.522
T1rho Corpus callosum	0.55 (0.42–0.68)	0.15	0.41	83.64 (71.2–92.2)	57.14 (18.4–90.1)	0.730

Area under receiver operating curve (AUC) test was used. TI rho: Time constant of spin-lattice relaxation in rotating frame; QSM: Quantitative Susceptibility mapping; DTI-MD: Diffusion tensor imaging-mean diffusivity; DTI FA: Diffusion tensor imaging- fractional anisotropy; SE: Standard error. Significant level, p < 0.05. Corpus Callosum included the following regions: Posterior, Mid Posterior, Central, Mid Anterior, and Anterior. Cingulate included these regions in both the left and right sides: Caudal Anterior, Posterior, Rostral Anterior, and Isthmus.

severe dementia," several brain regional volumes showed significant discriminatory power, including the hippocampus, thalamus, putamen, amygdala, corpus callosum, and cingulate. Additionally, various advanced neuroimaging biomarkers showed significant discriminatory ability. These included DTI-MD in the cuneus, cingulate, amygdala, hippocampus, corpus callosum, caudate, and thalamus; QSM in the caudate and putamen; and T1rho in the thalamus and hippocampus.

We found that increased amyloid burden $(A\beta+)$ was significantly associated with alterations in several imaging biomarkers across multiple brain regions. However, biomarkers indicative of atrophy and reduced microstructural integrity, specifically, volumes of the hippocampus, thalamus,

amygdala, cingulate, putamen, and corpus callosum volumes, and DTI-MD in the hippocampus, corpus callosum, cuneus, and cingulate demonstrated high diagnostic accuracy (AUC \geq 0.80), with hippocampal volumetry and hippocampal DTI-MD showing excellent performance (AUC > 0.90). These findings are consistent with previous studies ^{38–40} and underscore the central role of hippocampal degeneration and white matter disruption in the early and later stages of AD. In contrast, imaging biomarkers in the thalamus, caudate, putamen, and amygdala showed only fair to poor diagnostic performance (AUC = 0.79–0.50), suggesting that pathological changes in these regions may be less specific to AD, occur later in its progression, or may be less sensitively detected by these imaging metrics.

Reduced volumes in the hippocampus, thalamus, amygdala, cingulate, putamen, and corpus callosum and elevated DTI-MD reflect neuronal loss, diminished tissue integrity and overall progression of AD, 41,42 while lower DTI-FA in the amygdala and corpus callosum indicates compromised white matter integrity. We observed regionally divergent patterns, with more pronounced microstructural alterations in the hippocampus and cuneus compared to subcortical regions such as the thalamus and putamen, and atrophy in certain regions as indicated above. This likely reflects the characteristic progression of AD pathology, which typically begins in the transentorhinal regions (including the entorhinal cortex and hippocampus) before spreading to limbic structures (e.g., thalamus, amygdala, cingulate), neocortical areas (e.g., cuneus), and eventually the basal ganglia (e.g., putamen). 43,44

While hippocampal atrophy as one of the strongest single metrics for distinguishing between Aβ- and Aβ+ groups is a known sign of AD, it is not specific to the disease and can be observed in other neurodegenerative and non-neurodegenerative disorders. 43-45 In contrast, DTI-MD in the hippocampus also another strongest single metric for distinguishing between Aβ- and Aβ+ groups in our study is sensitive to microstructural white matter alterations and shows promise for detecting AD even in its early stages. 46 Although DTI-MD is also not entirely specific, it demonstrates greater discriminatory power than hippocampal volume alone. 47 Our study shows that combining DTI-MD and hippocampal volumetry increases diagnostic accuracy by 2.1%, suggesting that integrating T1-weighted MRI and DTI-MD offers a more effective biomarker strategy for AD detection. This combined approach could facilitate earlier and more accurate diagnosis, inform prognosis, and support personalized management strategies. Furthermore, incorporating these sensitive imaging biomarkers into clinical practice and research, particularly within the ATN (IVS) framework, could improve monitoring of disease progression and evaluating therapeutic interventions cost-effectively.

Atrophy of the hippocampus, thalamus, amygdala, cingulate, putamen, and corpus callosum and microstructural changes in the cuneus, cingulate, and amygdala reliably distinguished between early cognitive impairment and more advanced dementia, supporting their relevance for tracking disease progression. ⁴⁸ Imaging biomarkers identified in the amyloid-based classification model (using PET metrics) may be particularly sensitive to early and/or preclinical changes, whereas those highlighted by the clinical classification model reflect broader neurodegenerative processes associated with symptomatic cognitive decline. This distinction emphasizes the complementary value of imaging and clinical assessments, and the need to interpret biomarker findings within the context of disease stage or clinical question.

These findings underscore the importance of evaluating imaging biomarkers not only as diagnostic metrics but also as indicators of underlying biological processes, such as neuronal degeneration and white matter disruption. The contrasting associations observed across different regions suggest complex interactions between amyloid deposition, tau pathology, and neurodegeneration, which may manifest differently depending on the stage and anatomical spread of the disease. Identifying and targeting sensitive imaging biomarkers in key regions, particularly the transentorhinal and limbic areas, could be essential for accurate diagnosis of AD. Further, our findings highlight the complementary roles of other regional volumes, DTI-FA, QSM, and T1rho in the neuroimaging assessment of AD.

DTI-FA, which measures the directional coherence of water diffusion and reflects white matter integrity, was significantly reduced in the hippocampus and amygdala of $A\beta$ + subjects, indicating early microstructural disruption. Although its discriminative performance was fair, DTI-FA remains valuable for detecting subtle white matter changes that may precede overt atrophy and could serve as a sensitive marker for tracking disease progression or therapeutic response. 50

QSM, which quantifies tissue magnetic susceptibility and is sensitive to iron deposition and mineral alterations, showed higher values in the thalamus and putamen among $A\beta+$ subjects, with fair discriminative ability. QSM is emerging as a marker of brain iron accumulation, a process increasingly recognized for its interaction with $A\beta$ pathology,⁵¹ and offers unique mechanistic insights into the role of metal homeostasis and neuroinflammation in AD and may complement established biomarkers in multimodal imaging approaches.

T1rho, a marker of tissue macromolecular content and microenvironmental changes, was significantly reduced in the hippocampus of Aβ+ subjects and demonstrated fair diagnostic accuracy. Its sensitivity to biochemical and microenvironmental alterations makes it a promising tool for identifying prodromal AD, especially when combined with structural and diffusion imaging. 15 The integration of these modalities into multimodal imaging protocols holds potential for more comprehensive assessment, improved patient stratification, and the development of targeted therapeutic strategies in both clinical and research contexts. The seemingly paradoxical inverse relationship between T1rho values and $A\beta+$, particularly in the putamen and hippocampus, likely reflects the heterogeneous nature of the AD continuum within our cohort (A + T-N-, A + T + N-, and A + T+ N+). Pooling these groups, which represent different disease stages and pathological burdens, may obscure the expected positive correlation between T1rho and amyloid that is typically observed in later stages of the disease. It is conceivable that in the preclinical A+T-N- group, where amyloid is present, but tau pathology and neurodegeneration are absent, subtle compensatory mechanisms or a different molecular process might transiently decrease T1rho values. When this preclinical subgroup is combined

with more advanced A+T+N+ patients where the T1rho signal would be increased by both amyloid and tau pathology, the average effect across the entire $A\beta+$ cohort could be diluted or even reversed. Additionally, the complex interplay of different pathologies, such as the presence of iron, may influence T1rho in a region-specific manner that is not solely dependent on amyloid load.

Interestingly, LASSO regression analysis only showed a significant association with hippocampal volumetry. This outcome agrees with previous studies^{52–54} and underscore the complex and region-specific relationships between amyloid deposition and various aspects of brain structure, microstructure, and tissue properties. This suggests that while DTI-MD in the hippocampus effectively distinguishes between $A\beta$ + and $A\beta$ - groups, its direct association with amyloid positivity is weaker because amyloid deposition and neurodegeneration represent related but distinct pathological processes in AD. In our cohort, subjects included those with A + T - N -, A + T + N -, and A + T +N + along the AD continuum. Amyloid accumulation typically occurs early and may remain asymptomatic for years before tau pathology and neurodegeneration become evident. DTI-MD reflects microstructural damage and neuronal loss, which are more closely linked to tau pathology and progression to neurodegeneration. Therefore, many Aβ+ subjects, particularly those in the earlier stages, may not yet exhibit significant hippocampal neurodegeneration detectable by DTI-MD, while those with advanced pathology may be more likely to show pronounced changes. This heterogeneity may explain why DTI-MD can strongly distinguish Aβ+ from Aβ- groups overall, but its direct association with amyloid positivity is less robust.

The principal strength of this study lies in its comprehensive multimodal and multiparametric approach, integrating both established and novel imaging techniques to evaluate their effectiveness in detecting AD. By extending beyond the scope of previous research, this study provides a more robust assessment of these methods, with the potential to enhance diagnostic accuracy and deepen our understanding of AD-related brain changes. However, several limitations should be acknowledged. Firstly, the sample size is relatively small, particularly within the Aβ+ group, and the T + cohort was insufficient for meaningful subgroup analysis, partly due to the stringent inclusion and exclusion criteria employed. Secondly, as a cross-sectional study, it cannot account for longitudinal changes and thus cannot determine whether subjects with similar levels of AD pathology will exhibit comparable clinical symptoms over time. Future longitudinal studies involving larger and more diverse populations, and incorporating both clinical and biological classifications, are necessary to validate and extend these findings. Thirdly, the A β + group in this study predominantly comprises older subjects with MCI or AD, while the Aβ- group is younger and less cognitively impaired. This demographic and clinical disparity fundamentally

undermines the ability to attribute observed differences in imaging biomarkers such as hippocampal volumetry and DTI-MD exclusively to amyloid pathology. Instead, these differences may largely reflect the effects of advanced neurodegeneration and established disease, rather than early or preclinical amyloid-related changes. The confounding influence of age and cognitive impairment makes it difficult to disentangle whether the observed biomarker alterations are driven by amyloid deposition per se or by the broader spectrum of neurodegenerative changes associated with clinical progression. As such, the generalizability of our findings regarding the utility of these biomarkers for early detection is limited, and caution is warranted when interpreting these results. Fourthly, the differences in image processing and atlas registration between modalities, along with limited coverage for QSM and T1rho despite us using consistent ROI definitions via ANTs and FreeSurfer to mitigate inconsistencies, these factors introduce potential biases and constrain regional comparisons, requiring careful interpretation of multimodal findings. Finally, each imaging modality has inherent technical limitations that may have influenced the findings. Future studies should aim to recruit more demographically and clinically matched groups, particularly with greater representation of cognitively unimpaired Aβ+ subjects and employ longitudinal designs to clarify the specific contributions of amyloid pathology versus clinical severity to structural brain changes.

In conclusion, this study demonstrates that multimodal imaging biomarkers especially the volumes of the hippocampus, thalamus, amygdala, cingulate, putamen, corpus callosum and DTI-MD in the hippocampus, corpus callosum, and cuneus provide superior diagnostic accuracy for distinguishing subjects across the AD continuum. The complementary roles of DTI-FA, QSM, and T1rho offer additional insights into white matter integrity, iron accumulation, and biochemical changes, respectively. Incorporating these biomarkers into targeted, multimodal imaging protocols focused on key regions can further enhance detection, monitoring, and characterization of AD, ultimately supporting improved patient outcomes and the development of personalized therapeutic strategies.

Acknowledgements

The authors thank all the participants in the study.

ORCID iD

Chileka Chiyanika https://orcid.org/0000-0002-4744-1714

Ethical considerations

This study was conducted in accordance with the Helsinki declaration and approved by the Ethics Committee of the Joint Chinese University of Hong Kong—New Territories East Cluster Clinical Research Ethics Committee (REF NO. 2017.254).

Consent to participate

Written informed consent was obtained from all individual participants included in the study. For participants with cognitive impairment, consent was obtained from their legally authorized representatives.

Consent for publication

Consent for publication of images in this article was obtained from the participants and /or their legal guardians.

Author contribution(s)

Chileka Chiyanika: Conceptualization; Data curation; Methodology; Validation; Visualization; Writing – original draft. **Nga Yan Chan:** Data curation; Methodology; Software; Writing – review & editing.

Lisa Wing Chi Au: Investigation; Methodology; Supervision; Validation; Writing – review & editing.

Weitian Chen: Data curation; Writing – review & editing.

Sirong Chen: Data curation; Writing - review & editing.

Eric Yim Lung Leung: Data curation; Investigation; Methodology; Validation; Writing – review & editing.

Chi Lai Ho: Data curation; Investigation; Methodology; Validation; Writing – review & editing.

Yuan Cai: Data curation; Investigation; Methodology; Validation; Writing – review & editing.

Ho Ko: Data curation; Investigation; Methodology; Validation; Writing – review & editing.

Qianyun Chen: Data curation; Writing – review & editing. **Winnie Chu:** Investigation; Methodology; Supervision; Writing – review & editing.

Vincent Chung Tong Mok: Investigation; Methodology; Supervision; Validation.

Jill Abrigo: Conceptualization; Data curation; Investigation; Methodology; Supervision; Writing – review & editing.

Funding

The authors received no financial support for the research, authorship, and/or publication of this article.

Declaration of conflicting interests

The authors declared no potential conflicts of interest with respect to the research, authorship, and/or publication of this article.

Data availability statement

The raw data is available on request from the corresponding author.

Supplemental material

Supplemental material for this article is available online.

References

 World Health Organization. Global status report on the public health response to dementia, https://www.who.int/publications/ i/item/9789240033245 (2021, accessed 15 March 2024).

- Alzheimer's Association. Alzheimer's disease facts and figures. Alzheimers Dement 2016; 12: 459–509.
- 3. Prince M, Wimo A, Guerchet M, et al. World Alzheimer Report 2015. The global impact of dementia: An analysis of prevalence, incidence, cost and trends. London: Alzheimer's Disease International, 2015.
- 4. Patterson C. World Alzheimer Report 2018. The state of the art of dementia research: new frontiers. London: Alzheimer's Disease International, 2018.
- 5. Alzheimer's Association. 2023 Alzheimer's disease facts and figures. *Alzheimers Dement* 2023; 19: 1598–1695.
- Bateman RJ, Xiong C, Benzinger TL, et al. Clinical and biomarker changes in dominantly inherited Alzheimer's disease. N Engl J Med 2012; 367: 795–804.
- Jack CR Jr, Bennett DA, Blennow K, et al. NIA-AA research framework: toward a biological definition of Alzheimer's disease. Alzheimers Dement 2018; 14: 535–562.
- 8. Cohen AD, Landau SM, Snitz BE, et al. Fluid and PET biomarkers for amyloid pathology in Alzheimer's disease. *Mol Cell Neurosci* 2019; 97: 3–17.
- 9. Meyer P, McSweeney M, Gonneaud J, et al. PET Amyloid imaging across the Alzheimer's disease spectrum: from disease mechanisms to prevention. *Prog Mol Biol Transl Sci* 2019; 165: 63–106.
- Hampel H, O'Bryant SE, Molinuevo JL, et al. Blood-based biomarkers for Alzheimer disease: mapping the road to the clinic. *Nat Rev Neurol* 2018; 14: 639–652.
- 11. Landau SM, Breault C, Joshi AD, et al. Amyloid-β imaging with Pittsburgh compound B and florbetapir: comparing radiotracers and quantification methods. *J Nucl Med* 2013; 54: 70–77.
- 12. Cohen AD, Rabinovici GD, Mathis CA, et al. Using Pittsburgh compound B for in vivo PET imaging of fibrillar amyloid-beta. *Adv Pharmacol* 2012; 64: 27–81.
- 13. Kantarci K, Murray ME, Schwarz CG, et al. White-matter integrity on DTI and the pathologic staging of Alzheimer's disease. *Neurobiol Aging* 2017; 56: 172–179.
- Cogswell PM, Wiste HJ, Senjem ML, et al. Associations of quantitative susceptibility mapping with Alzheimer's disease clinical and imaging markers. *Neuroimage* 2021; 224: 117433.
- 15. Haris M, Yadav SK, Rizwan A, et al. T1rho MRI and CSF biomarkers in diagnosis of Alzheimer's disease. *Neuroimage Clin* 2015; 7: 598–604.
- Borthakur A, Sochor M, Davatzikos C, et al. T1ρ MRI of Alzheimer's disease. *Neuroimage* 2008; 41: 1199–1205.
- Chan SS, Lam LC, Tam CW, et al. Prevalence of clinically significant depressive symptoms in an epidemiologic sample of community-dwelling elders with milder forms of cognitive impairment in Hong Kong SAR. *Int J Geriatr Psychiatry* 2008; 23: 611–617.
- 18. Wei Y, Huang L, Chen C, et al. Subjective cognitive decline in the community is affected at multiple aspects of mental health and life quality: a cross-sectional study of the community medicine of Keelung Chang Gung Memorial Hospital. *Dement Geriatr Cogn Disord Extra* 2019; 9: 152–162.

- McKhann GM, Knopman DS, Chertkow H, et al. The diagnosis of dementia due to Alzheimer's disease: recommendations from the National Institute on Aging-Alzheimer's Association workgroups on diagnostic guidelines for Alzheimer's disease.
 Alzheimers Dement 2011; 7: 263–269.
- 20. Morris JC. The clinical dementia rating (CDR) current version and scoring rules. *J Neurol* 1993; 43: 2412–2414.
- Liu W, Au LWC, Abrigo J, et al. MRI-based Alzheimer's disease-resemblance atrophy index in the detection of preclinical and prodromal Alzheimer's disease. *Aging (Albany NY)* 2021; 13: 13496.
- Jacobs HI, Hedden T, Schultz AP, et al. Structural tract alterations predict downstream tau accumulation in amyloid-positive older individuals. *Nat Neurosci* 2018; 21: 424–431.
- Li W, Avram AV, Wu B, et al. Integrated Laplacian-based phase unwrapping and background phase removal for quantitative susceptibility mapping. NMR Biomed 2014; 27: 219–227.
- Li W, Wu B, Batrachenko A, et al. Differential developmental trajectories of magnetic susceptibility in human brain gray and white matter over the lifespan. *Hum Brain Mapp* 2014; 35: 2698–2713.
- Wei H, Dibb R, Zhou Y, et al. Streaking artifact reduction for quantitative susceptibility mapping of sources with large dynamic range. *NMR Biomed* 2015; 28: 1294–1303.
- 26. Haris M, Singh A, Cai K, et al. T1rho (T1ρ) MR imaging in Alzheimer's disease and Parkinson's disease with and without dementia. *J Neurol* 2011; 258: 380–385.
- Li X, Morgan PS, Ashburner J, et al. The first step for neuroimaging data analysis: DICOM to NIfTI conversion. *J Neurosci Methods* 2016; 264: 47–56.
- Jenkinson M. BET2: MR-based estimation of brain, skull and scalp surfaces. In: Eleventh Annual Meeting of the Organization for Human Brain Mapping, Toronto, Canada, 11 June-15 June 2005, article no. 10030066593. Japan: CiNii.
- Najm M, Kuang H, Federico A, et al. Automated brain extraction from head CT and CTA images using convex optimization with shape propagation. *Comput Methods Programs Biomed* 2019; 176: 1–8.
- 30. Destrieux C, Fischl B, Dale A, et al. Automatic parcellation of human cortical gyri and sulci using standard anatomical nomenclature. *Neuroimage* 2010; 53: 1–15.
- 31. Fischl B, Salat DH, Busa E, et al. Whole brain segmentation: automated labeling of neuroanatomical structures in the human brain. *Neuron* 2002; 33: 341–355.
- 32. Jack CR Jr, Wiste HJ, Weigand SD, et al. Defining imaging biomarker cut points for brain aging and Alzheimer's disease. *Alzheimers Dement* 2017; 13: 205–216.
- Jack CR Jr, Andrews JS, Beach TG, et al. Revised criteria for diagnosis and staging of Alzheimer's disease: Alzheimer's Association workgroup. *Alzheimers Dement* 2024; 20: 5143–5169.

- Maass A, Landau S, Baker SL, et al. Comparison of multiple tau-PET measures as biomarkers in aging and Alzheimer's disease. *Neuroimage* 2017; 157: 448–463.
- Insel PS, Mormino EC, Aisen PS, et al. Neuroanatomical spread of amyloid β and tau in Alzheimer's disease: implications for primary prevention. *Brain Commun* 2020; 2: fcaa007.
- Jagust WJ, Landau SM, Shaw LM, et al. Relationships between biomarkers in aging and dementia. *J. Neurol* 2009; 73: 1193–1199.
- Nahm FS. Receiver operating characteristic curve: overview and practical use for clinicians. *Korean J Anesthesiol* 2022; 75: 25–36.
- Gerischer LM, Fehlner A, Köbe T, et al. Combining viscoelasticity, diffusivity and volume of the hippocampus for the diagnosis of Alzheimer's disease based on magnetic resonance imaging. *Neuroimage Clin* 2018; 18: 485–493.
- Park HY, Suh CH, Heo H, et al. Diagnostic performance of hippocampal volumetry in Alzheimer's disease or mild cognitive impairment: a meta-analysis. *Eur Radiol* 2022; 32: 6979–6991.
- Lu C, Ng S, Weng Y, et al. Alterations of diffusion tensor MRI parameters in the brains of patients with Parkinson's disease compared with normal brains: possible diagnostic use. *Eur Radiol* 2016; 26: 3978–3988.
- De Leon MJ, DeSanti S, Zinkowski R, et al. MRI And CSF studies in the early diagnosis of Alzheimer's disease. *J Intern* Med 2004; 256: 205–223.
- 42. Colliot O, Chételat G, Chupin M, et al. Discrimination between Alzheimer disease, mild cognitive impairment, and normal aging by using automated segmentation of the hippocampus. *Radiology* 2008; 248: 194–201.
- Fujioka M, Nishio K, Miyamoto S, et al. Hippocampal damage in the human brain after cardiac arrest. Cerebrovasc Dis 2000; 10: 2–7.
- 44. Agartz I, Momenan R, Rawlings RR, et al. Hippocampal volume in patients with alcohol dependence. *Arch Gen Psychiatry* 1999; 56: 356–363.
- Abernethy LJ, Palaniappan M and Cooke RW. Quantitative magnetic resonance imaging of the brain in survivors of very low birth weight. *Arch Dis Child* 2002; 87: 279–283.
- Palesi F, Vitali P, Chiarati P, et al. DTI And MR volumetry of hippocampus-PC/PCC circuit: in search of early micro- and macrostructural signs of Alzheimer's disease. *Neurol Res Int* 2012; 2012: 517876.
- Müller MJ, Greverus D, Weibrich C, et al. Diagnostic utility of hippocampal size and mean diffusivity in amnestic MCI. *Neurobiol Aging* 2007; 28: 398–403.
- Chouliaras L and O'Brien JT. The use of neuroimaging techniques in the early and differential diagnosis of dementia. *Mol Psychiatry* 2023; 28: 4084–4097.
- Acosta-Cabronero J, Alley S, Williams GB, et al. Diffusion tensor metrics as biomarkers in Alzheimer's disease. *PLoS One* 2012; 7: e49072.

- Nir TM, Jahanshad N, Villalon-Reina JE, et al. Effectiveness of regional DTI measures in distinguishing Alzheimer's disease, MCI, and normal aging. *Neuroimage Clin* 2013; 3: 180–195.
- Ayton S, Fazlollahi A, Bourgeat P, et al. Cerebral quantitative susceptibility mapping predicts amyloid-β-related cognitive decline. *Brain* 2017; 140: 2112–2119.
- 52. Ten Kate M, Barkhof F, Visser PJ, et al. Amyloid-independent atrophy patterns predict time to progression to dementia in mild cognitive impairment. *Alzheimers Res Ther* 2017; 9: 73.
- 53. Melah KE, Lu SY, Hoscheidt SM, et al. Cerebrospinal fluid markers of Alzheimer's disease pathology and microglial activation are associated with altered white matter microstructure in asymptomatic adults at risk for Alzheimer's disease. *J Alzheimers Dis* 2016; 50: 873–886.
- 54. Wu X, Wu Y, Geng Z, et al. Asymmetric differences in the gray matter volume and functional connections of the amygdala are associated with clinical manifestations of Alzheimer's disease. *Front Neurosci* 2020; 14: 602.